Memorias del 2022 Congreso Nacional de Control Automático
12-14 de Octubre, 2022. Tuxtla Gutiérrez, México.

Low-cost DSP-based vibration data acquisition system for bearing fault detection in electric motors

F.J. Villalobos-Piña * **R. Alvarez-Salas** **
M.A. Gonzalez-Garcia *** **J.A. Reyes-Malanche** ****
C.H. Saucedo-Zarate * **L.A. Gonzalez-Murillo** **

* *TecNM/Instituto Tecnológico de Aguascalientes, Aguascalientes, Ags., 20256 México (e-mail: fvillalobos@mail.ita.mx, carloshum777@hotmail.com).*
** *Facultad de Ingeniería, Universidad Autónoma de San Luis Potosí, San Luis Potosí, S.L.P., 78290 Mexico (e-mail: ralvarez@uaslp.mx, luis.murillo@uaslp.mx).*
*** *CONACYT / Facultad de Ingeniería, Universidad Autónoma de San Luis Potosí, San Luis Potosí, S.L.P., 78290 México (e-mail: mgonzale@uaslp.mx).*
**** *Universidad Tecnológica de Aguascalientes, Aguascalientes, Ags., 20196 México (e-mail: josue.malanche@utags.edu.mx).*

Abstract: This paper presents a low-cost DSP-based vibration data acquisition system with a high data storage capacity for fault detection in electric motors. An outer race bearing fault detection case study for a three-phase induction machine using vibration signals provided by the DSP-based acquisition system from a test rig is detailed. The fault detection scheme is performed based on Fast Fourier Transform (FFT) and Discrete Wavelet Transform (DWT).

Keywords: Fault Detection, Induction Motor, Mechanical Faults, Wavelet, MRA Analysis

1. INTRODUCTION

The electric machines represent the principal source of movement in the industrial sector (Trigeassou (2011)), (Toliyat et al. (2013)), (Verde et al. (2013)). The induction machine (IM) is widely recognized as the workhorse of the industry (Mujica and Espinoza-Pérez (2014)). This kind of machine has a top exclusive position in converting electric to mechanical energy, being responsible for almost 90% of all the energy consumption of the electric motors in the industry.

Fault detection techniques for three-phase electric machines have been extensively studied in the last several years to detect faults early and compensate for their adverse effects during scheduling maintenance to avoid unnecessary costs. The fault distribution within machine subassemblies is reported in many reliable survey papers. A summary classification identifies four classes: bearing faults, stator-related faults, rotor-related faults, and other faults (cooling, connection, terminal boxes, and power converter faults). Depending on the type and size machine bearing fault distribution among all faults varies from about 40% to about 90% from large to small machines. Vibration signals are typically used to detect the presence of mechanical bearing faults. In most situations, diagnostic methods based on analysis of mechanical fault signals have proved their effectiveness for single defects (Immovilli et al. (2009)). Hence, early bearing damage detection can significantly help reduce the costs that these downtimes will entail. The reasons for a bearing to fail are manifold. A well-lubricated and properly installed bearing under appropriate working conditions will not usually degrade before the end of its expected lifetime (Zoubek et al. (2008)).

The electrical stator faults represent a significant percentage of IM faults. Included in this category, there are the coil faults like inter-turn short-circuits and core magnetic faults (Cruz and Cardoso (2001)). Unfortunately, the IM can fail due to other mechanisms; for example, squirrel cage broken rotor bars and rotor end ring short-circuit faults. These kinds of faults are due to different stress mechanisms that act on the rotor (Cruz and Cardoso. (1999)), (Bellini et al. (2008a)), (Bellini et al. (2008b)). Due to the increment of efficiency and development of new aero-spacial materials applied to electric isolation in

⋆ This work was partially supported by TecNM/Instituto Tecnológico de Aguascalientes and UASLP-CA-246 Sistemas Eléctromecánicos y Energía Sustentable.

electric motors, the machines' size has been reduced, and their mechanical stress has increased. This stress produces bearing damages, eccentricity, and shaft deviation problems. The most common mechanical faults are inner and outer race bearing faults, static or dynamic eccentricity faults, and unbalanced rotor shaft faults.

This paper presents a bearing outer race fault detection scheme based on FFT and DWT using vibration signals. This signal is obtained with a low-cost DSP-based data acquisition system with high storage capacity.

2. BEARING FAULT DETECTION

A fault can be defined as a non-permitted deviation of the process parameters. There are three kinds of faults types: abrupt faults, incipient faults and intermittent faults. In recent years, it has been reported the induction machines fault distribution is: bearing faults (69%), stator faults (21%), rotor broken bars or end ring rotor short circuit faults (7%), shaft and couple faults (3%) (Elbouchikhi et al. (2016)), (Pacheco-Chérrez et al. (2022)), (Tiwari and Upadhyay (2021)).

The bearing fault in induction machines is one of the most common faults in this kind of machine (Bellini et al. (2008b)). Most of electric machines use balls or rolling elements in bearings. A bearing consists of two concentric rings, one called inner race and the other outer race, both are depicted in the Fig. 1 with a group of rotating elements located between this concentric rings.

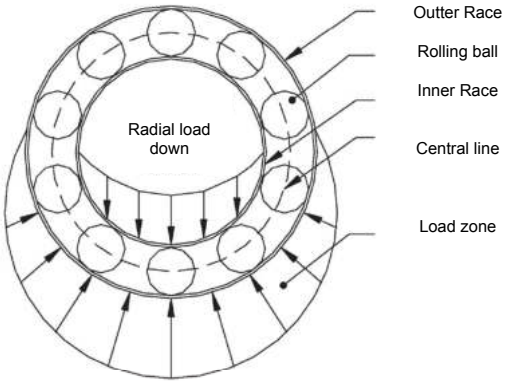

Fig. 1. Bearing structure.

Under normal operation conditions with unbalanced loads and good alignment, this kind of fault can occur. This fault increases the vibration levels. It is also possible that the fire appears when small pieces of the bearing reach the rolling elements between the inner and outer race. An example of damaged inner and outer races is shown in the Fig. 2.

The bearing fault can be caused by:

- Pollution or corrosion is produced by erosion caused by the abrasion of small particles, water, or acid.

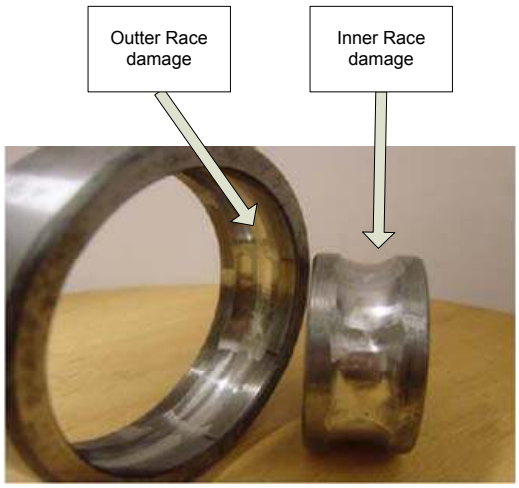

Fig. 2. Damaged inner and outer races (Silva and Cardoso. (2005)).

- Inappropriate lubrication.
- Inappropriate installation.

The bearing fault spectra signatures are described in (Silva and Cardoso. (2005)). Moreover, the mechanical characteristic frequency f_{car}, when the outer race is fixed, is classified into four types:

- Outer Race f_{bor} (Hz):

$$f_{bor} = \frac{N_b}{2} f_{rotor} \left[1 - \frac{D_b}{D_c} \cos\beta\right] \tag{1}$$

- Inner Race f_{bir} (Hz):

$$f_{bir} = \frac{N_b}{2} f_{rotor} \left[1 + \frac{D_b}{D_c} \cos\beta\right] \tag{2}$$

- Balls f_{bba} (Hz):

$$f_{bba} = \frac{D_c}{2D_b} f_{rotor} \left[1 - \left(\frac{D_b}{D_c} \cos\beta\right)^2\right] \tag{3}$$

- Cage f_{bca} (Hz):

$$f_{bca} = \frac{f_{rotor}}{2} \left[1 - \frac{D_b}{D_c} \cos\beta\right] \tag{4}$$

The rolling element in the bearing is presented in the Fig. 3. D_b is the ball diameter, D_c is the pitch diameter, N_b is the number of rolling elements, β is the ball contact angle (zero for rollers), and f_{rotor} is the induction motor rotor frequency.

3. FFT AND DWT

The fault signatures from the induction motor vibration signals are analyzed using the FFT base two with time decimation and the DWT with three mother wavelets, Haar, Daubechies, and Coiflet.

The DWT allows a multi-resolution analysis (MRA) of the vibration signals, as depicted in Fig. 4. The MRA

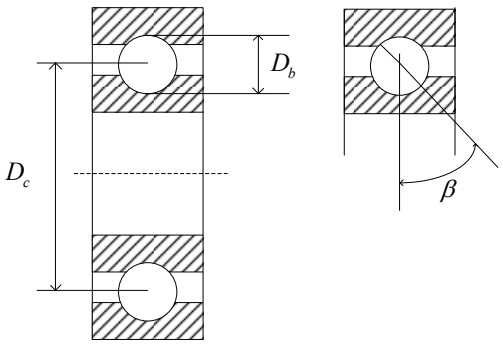

Fig. 3. Rolling elements geometry.

consists in creating an approximation component using scaling function (a lowpass filter l(n)) and detail components using wavelet functions (highpass filters h(n)). A series of approximations of a signal is created, each differing in resolution by a factor of 2. The detail components contain the difference between adjacent approximations (Walker (2008)).

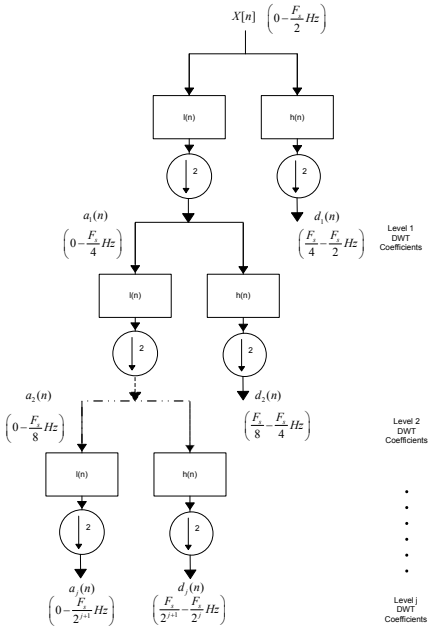

Fig. 4. Wavelet multi-resolution analysis.

4. VIBRATION DATA ACQUISITION SYSTEM

A low-cost vibration data acquisition system was developed. The system consists on 3-axis accelerometer (Analog Devices ADXL335) interconnected to a DSP (Microchip dsPIC30F4011) that runs at 117.9648 Mhz. The data are stored on a high speed microSD flash memory unit. The block diagram of the system is depicted in Fig. 5.

All the necessary commands to perform the data management in the microSD memory unit were implemented by

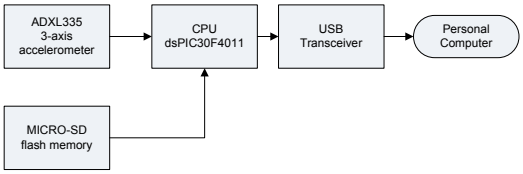

Fig. 5. Block diagram of the vibration data acquisition system with high storage capacity.

software in the DSP. The DSP algorithm can manage the newest high-capacity memory formats like SDHC. This format supports cards with capacities up to 32 GB. For simplicity, the present design it was used an 8 GB memory and is depicted in Fig. (6).

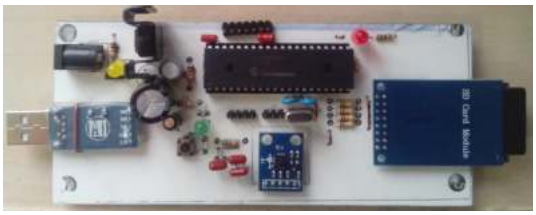

Fig. 6. Vibration data acquisition system with a high data storage capacity.

The data acquisition system installed on the induction motor is shown in Fig. (6) and the mounting detail is shown in the figure(7).

The acquired information is downloaded to a PC using a high speed USB interface and a Delphi-based software.

The computer program has the following features:

- Download the acquired vibration data.
- Modify the DSP sampling frequency (up to 25 Khz).
- Acquire simultaneously three acceleration signals (X, Y, and Z-axis), three motor line currents (A, B and C phase) and shaft angular position of the rotor.
- Store in disk the data for post-processing.

5. CASE STUDY

A group of four bearings, one healthy and three faulty, of a $\frac{1}{4}$ HP 220 V 4 poles three-phase induction motor were used to perform the experiments.

The three faulty bearings were altered to introduce different outer race faults as follows:

- Bearing with one $\frac{1}{8}$ in hole.
- Bearing with two $\frac{1}{8}$ in holes.
- Bearing with three $\frac{1}{8}$ in holes.

The four bearings were changed for each test in the induction machine rotor shaft (Fig. 8). The vibration signal given by the accelerometer was acquired using a sampling frequency $F_s = 5$ Khz and 8192 samples were taken for

Fig. 7. The vibration data acquisition system mounted on the induction motor.

each case. The bearing characteristics of the induction motor are shown in table 1.

Table 1. Three-phase induction motor bearing parameters.

Parameter	Size (mm)
Rolling elements diameter D_b	7.30
Pitch diameter D_c	28.5
Number of rolling elements N_b	8

Fig. 8. Induction machine rotor shaft with a hole in the outer race bearing.

The vibration signal spectra obtained applying the FFT to the four case studies (one healthy and three faulty scenarios) at 1800 RPM are shown in the Fig. 9, the frequency of the outer race fault is obtained with equation (1) and it is $F_{bor} = 86.7836\ Hz$.

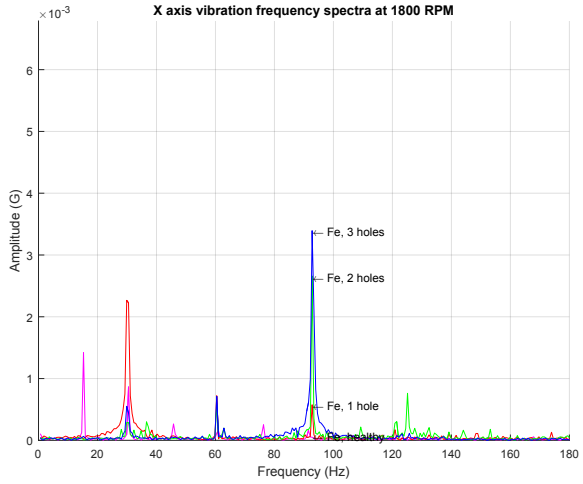

Fig. 9. Vibration signal frequency spectra at 1800 RPM.

In Fig. 10, the vibration signal spectra obtained for the four case studies at 1500 RPM is presented, the frequency of the outer race fault is $F_{bor} = 74.38596\ Hz$.

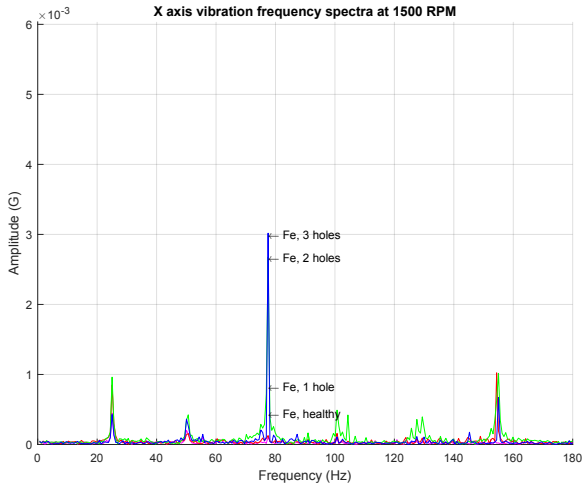

Fig. 10. Vibration signal frequency spectra at 1500 RPM.

Fig. 11 shows the vibration signal spectra obtained for the four case studies at 1200 RPM, the frequency of the outer race fault is $F_{bor} = 59.5088\ Hz$.

The RMS values of the level 1 Haar wavelet coefficients obtained from vibration signal for the four scenarios at 1800 RPM is shown in Table 2, the band number 5 show the RMS magnitude change due to the bearing fault. The same results are presented in Tables 3, 4, and 5 for using Daubechies 4, Daubechies 6, and Coiflet wavelets, respectively.

An increment in the spectrum magnitudes, obtained with FFT, was observed as the number of holes in the bearings was increased. Meanwhile, the best fault

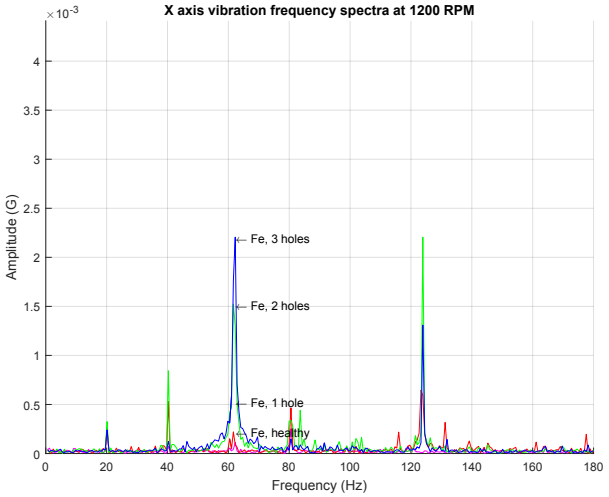

Fig. 11. Vibration signal frequency spectra at 1200 RPM.

Table 2. RMS values of the Haar wavelet coefficients at 1800 RPM.

Level	Band	Healthy	1 hole	2 holes	3 holes
1	1250.0-2500.0	0.0003	0.0009	0.0011	0.0012
2	625.0-1250.0	0.0003	0.0010	0.0018	0.0024
3	312.5-625.0	0.0004	0.0015	0.0037	0.0054
4	156.3-312.5	0.0008	0.0028	0.0071	0.0080
5	78.1-156.3	0.0020	0.0054	0.0113	0.0134
6	39.1-78.1	0.0041	0.0118	0.0119	0.0148
7	19.5-39.1	0.0083	0.0217	0.0048	0.0045
8	9.8-19.5	0.0117	0.0077	0.0058	0.0066
9	4.9-9.8	0.0046	0.0120	0.0027	0.0029
10	2.4-4.9	0.0065	0.0020	0.0025	0.0033
11	1.2-2.4	0.0018	0.0020	0.0013	0.0014
12	0.6-1.2	0.0038	0.0053	0.0008	0.0003
13	0.3-0.6	0.0065	0.0010	0.0040	0.0008

Table 3. RMS values of the Db4 wavelet coefficients at 1800 RPM.

Level	Band	Healthy	1 hole	2 holes	3 holes
1	1250.0-2500.0	0.0093	0.0416	0.0348	0.0228
2	625.0-1250.0	0.0050	0.0313	0.0205	0.0130
3	312.5-625.0	0.0039	0.0182	0.0130	0.0070
4	156.3-312.5	0.0047	0.0102	0.0080	0.0050
5	78.1-156.3	0.0031	0.0117	0.0052	0.0046
6	39.1-78.1	0.0134	0.0055	0.0041	0.0033
7	19.5-39.1	0.0083	0.0249	0.0042	0.0030
8	9.8-19.5	0.0033	0.0113	0.0119	0.0138
9	4.9-9.8	0.0017	0.0040	0.0129	0.0157
10	2.4-4.9	0.0007	0.0024	0.0068	0.0072
11	1.2-2.4	0.0003	0.0013	0.0034	0.0055
12	0.6-1.2	0.0003	0.0009	0.0013	0.0018
13	0.3-0.6	0.0003	0.0009	0.0009	0.0009

detection with DWT was obtained using the Haar wavelet for the different mechanical bearing fault case studies.

6. CONCLUSION

According to experimental results, the DSP-based vibration data acquisition system was suitable for implementing fault detection schemes in electric motors. A significant advantage of this system is its capacity to store a high volume of data for a detailed offline analysis.

Table 4. RMS values of the Db6 wavelet coefficients at 1800 RPM.

Level	Band	Healthy	1 hole	2 holes	3 holes
1	1250.0-2500.0	0.0161	0.0323	0.0569	0.0282
2	625.0-1250.0	0.0073	0.0396	0.0272	0.0164
3	312.5-625.0	0.0051	0.0233	0.0195	0.0100
4	156.3-312.5	0.0043	0.0147	0.0124	0.0060
5	78.1-156.3	0.0023	0.0112	0.0075	0.0032
6	39.1-78.1	0.0138	0.0054	0.0045	0.0022
7	19.5-39.1	0.0080	0.0257	0.0041	0.0031
8	9.8-19.5	0.0033	0.0105	0.0115	0.0132
9	4.9-9.8	0.0014	0.0035	0.0137	0.0165
10	2.4-4.9	0.0006	0.0024	0.0064	0.0066
11	1.2-2.4	0.0003	0.0012	0.0033	0.0057
12	0.6-1.2	0.0003	0.0009	0.0012	0.0015
13	0.3-0.6	0.0003	0.0009	0.0009	0.0009

Table 5. RMS values of the Cofilet wavelet coefficients at 1800 RPM.

Level	Band	Healthy	1 hole	2 holes	3 holes
1	1250.0-2500.0	0.0175	0.0439	0.0665	0.0220
2	625.0-1250.0	0.0091	0.0427	0.0362	0.0137
3	312.5-625.0	0.0050	0.0263	0.0226	0.0079
4	156.3-312.5	0.0051	0.0150	0.0139	0.0154
5	78.1-156.3	0.0030	0.0127	0.0076	0.0045
6	39.1-78.1	0.0131	0.0059	0.0046	0.0032
7	19.5-39.1	0.0080	0.0244	0.0040	0.0031
8	9.8-19.5	0.0035	0.0112	0.0118	0.0137
9	4.9-9.8	0.0015	0.0039	0.0130	0.0157
10	2.4-4.9	0.0007	0.0024	0.0066	0.0072
11	1.2-2.4	0.0003	0.0013	0.0034	0.0055
12	0.6-1.2	0.0003	0.0009	0.0013	0.0018
13	0.3-0.6	0.0003	0.0009	0.0009	0.0009

ACKNOWLEDGEMENTS

This work was partially supported by DEPI-ITA-TecNm (Departamento de Posgrado e Investigación - Instituto Tecnológico de Aguascalientes/Tecnológico Nacional de México).

REFERENCES

Bellini, A., Filippetti, F., Tassoni, C., and Capolino, A.G. (2008a). Advances in diagnostic techniques for induction machines. *IEEE Transactions on Industrial Electronics*, 55(12), 4109–4126.

Bellini, A., Immovilli, F., Rubini, R., and Tassoni, C. (2008b). Diagnosis of bearing faults in induction machines by vibration or current signals: a critical comparison. *IEEE Transaction on Industrial Electronics*, 5, 1–8.

Cruz, S.M.A. and Cardoso., A.J.M. (1999). Rotor cage fault diagnosis in three-phase induction motors by extended Park's vector approach. *Industry Applications Conference*, Vol. 3, 1929–1934.

Cruz, S.M.A. and Cardoso, A.J.M. (2001). Stator winding fault diagnosis in three-phase synchronous and asyn-

chronous motors, by the extended Park's vector approach. *IEEE Transcations on Industry Applications*, 37(5), 1227–1233.

Elbouchikhi, E., Choqueuse, V., and Benbouzid, M. (2016). Induction machine bearing faults detection based on a multi-dimensional music algorithm and maximum likelihood estimation. *ISA Transactions*, 63, 413–424.

Immovilli, F., Cocconcelli, M., Bellini, A., and Rubini, R. (2009). Detection of generalized-roughness bearing fault by spectral-kurtosis energy of vibration or current signals. *IEEE Transactions on Industrial Electronics*, 56(11), 4710–4717.

Mujica, H. and Espinoza-Pérez, G. (2014). Control no lineal basado en pasividad de motores de inducción para alto desempeño dinámico. *Revista Iberoamericana de Automática e Informática industrial*, 11, 32–43.

Pacheco-Chérrez, J., Fortoul-Díaz, J.A., Cortés-Santacruz, F., Aloso-Valerdi, L.M., and Ibarra-Zarate, D.I. (2022). Bearing fault detection with vibration and acoustic signals: Comparison among different machine learning classification methods. *Engineering Failure Analysis*, 139.

Silva, J.L.H. and Cardoso., A.J.M. (2005). Bearing failures diagnosis in three-phase induction motors by extended Park's vector approach. *IECON 31st. Annual Conference of IEEE*, 2591–2596.

Tiwari, P. and Upadhyay, S.H. (2021). Novel self-adaptative vibration signal analysis: Concealed component decomposition and its application in bearing fault diagnosis. *Journal of Sound and Vibration*, 502.

Toliyat, H., Nandi, S., Choi, S., and Meshing-Kelk, H. (2013). *Electrical Machines*. CRC Press. USA, 1 edition.

Trigeassou, J. (2011). *Electrical Machines Diagnosis*. Wiley USA, 1 edition.

Verde, C., Gentil, S., and Morales-Menéndez, R. (2013). *Monitoreo y diagnóstico automático de fallas en sistemas dinámicos*. Trillas México.

Walker, J. (2008). *A Primer on Wavelets and Their Scientific Applications*. Chapman & Hall/CRC, 2nd edition.

Zoubek, H., Villwock, S., and Pacas, M. (2008). Frequency response analysis for rolling-bearing damage diagnosis. *IEEE Transactions on Industrial Electronics*, 55(12), 4270–4275.